

A novel multiwavelength fluorescence image-guided surgery imaging system

D. Volpi^{*a}, I. D. C. Tullis^a, A. Laios^{b,c}, P. N. J. Pathiraja^{b,c,d}, K. Haldar^d, A. A. Ahmed^{b,c}, B. Vojnovic^a

^a Department of Oncology, Gray Institute for Radiation Oncology and Biology, University of Oxford, Old Road Campus Research Building, Oxford, OX3 7DQ, UK; ^b Nuffield Department of Obstetrics and Gynaecology, University of Oxford, Women's Centre, John Radcliffe Hospital, Oxford, OX3 9DU, UK; ^c Weatherall Institute of Molecular Medicine, University of Oxford, John Radcliffe Hospital, Oxford, OX3 9DS, UK; ^d Oxford University Hospitals NHS Trust, Churchill Hospital, Oxford, OX3 7LE, UK.

ABSTRACT

We describe the development and performance analysis of two clinical near-infrared fluorescence image-guided surgery (FIGS) devices that aim to overcome some of the limitations of current FIGS systems. The devices operate in a widefield-imaging mode and can work (1) in conjunction with a laparoscope, during minimally invasive surgery, and (2) as a hand-held, open surgery imaging system. In both cases, narrow-band excitation light, delivered at multiple wavelengths, is efficiently combined with white reflectance light. Light is delivered to $\sim 100 \text{ cm}^2$ surgical field at 1-2 mW/cm² for white light and 3-7 mW/cm² (depending on wavelength) of red - near infrared excitation, at a typical working distance of 350 mm for the hand-held device and 100 mm for the laparoscope. A single, sensitive, miniaturized color camera collects both fluorescence and white reflectance light. The use of a single imager eliminates image alignment and software overlay complexity. A novel filtering and illumination arrangement allows simultaneous detection of white reflectance and fluorescence emission from multiple dyes in real-time. We will present both fluorescence detection sensitivity modeling and practical performance data. We have demonstrated the efficiency and the advantages of the devices both pre-clinically and during live surgery on humans. Both the hand-held and the laparoscopic systems have proved to be reliable and beneficial in an ongoing clinical trial involving sentinel lymph node detection in gynecological cancers. We will show preliminary results using two clinically approved dyes, Methylene blue and indocyanine green. We anticipate that this technology can be integrated and routinely used in a larger variety of surgical procedures.

Keywords: Image-guided surgery, Fluorescence, Widefield imaging, Laparoscopy, Near infrared, Lymph nodes.

1. INTRODUCTION

Cancer is a leading cause of death worldwide. Despite the widespread use of radiotherapy and chemotherapy to treat certain types of cancer, the primary and most successful approach for treatment is surgery¹. This practice relies on the visual ability of the surgeon to detect and remove tumor tissue intra-operatively. As a result, one of the fundamental limitations of cancer surgery, and in particular of minimally invasive (keyhole) surgery, is that tumor tissue needs to be visually discriminated from the healthy tissue.

Fluorescence image-guided surgery (FIGS) has recently emerged as a complementary imaging technique to white light reflectance imaging and it aims to provide the surgeon with an extra tool to identify tissues of interest². This imaging modality is based on the use of clinically approved contrast agents that are excited in the visible – near infrared region of the electromagnetic spectrum. Contrast agents can be used to label tumor tissue³ or can be used in a non-specific manner to detect lymph nodes and, in particular, sentinel lymph nodes⁴. The near infrared (NIR) region of the electromagnetic spectrum has several advantages over the visible: these include higher penetration depths, lower scattering and lower tissue autofluorescence⁵. Moreover, the use of ‘invisible’ excitation light does not interfere with the visual operation

* davide.volpi@oncology.ox.ac.uk; phone +44 1865 617383

<http://users.ox.ac.uk/~atdgroup/>

field, which is still the surgeon's ultimate imaging tool. Some of the critical requirements of FIGS instrumentation include imaging in real time and simultaneous visualization of bright field (reflectance) and fluorescence emission.

The use of fluorescent tumor markers in human clinical surgery is in its infancy, although extensive pre-clinical studies are taking place⁶⁻⁹. Clinical applications, particularly in the case of keyhole surgery are, in general, hampered by the poor and often unknown light collection efficiencies of the optical instruments used: laparoscopes and endoscopes.

In the work presented here, we have characterized the optical performance of laparoscopes conventionally used for white-light imaging in the abdomen, where 10 mm diameter instruments are generally used. We have determined both the laparoscope aperture and its transmission in the visible and NIR spectral regions. We also present examples of clinical applications. In addition, we present results obtained with a widefield, open surgery, hand-held imaging device and use this as a 'standard' in deriving losses incurred by the use of a laparoscope. Both of these systems are novel, low-cost, miniaturized and explicitly designed for FIGS applications. Both share a common control unit and allow straightforward interchange of imaging heads, facilitating the use of FIGS in cases where a planned minimally invasive procedure proves inappropriate, requiring an open surgery approach.

The common control system is capable of exciting at numerous wavelengths, although the data presented here include only two excitation wavelengths. Imaging is performed with a single color camera that detects both white light reflectance images and fluorescence emission(s) simultaneously without the need for false color software overlays, commonly required when multiple cameras are used.

We predict the practical performance of the laparoscope from f/number and transmission measurement and by comparison with a well-characterized widefield imager. A clinical feasibility study involving lymph node detection in gynecological cancers has further validated these novel devices. One of the aims was to validate the concept of sentinel lymph nodes^{10,11} and to establish potential new applications with emerging tumor markers.

Although a number of devices for FIGS have been described in the past¹²⁻¹⁷, only few of them have gone forward to clinical application. Some of the limitations of these devices include significant volume and weight, not compatible with hand-held operation^{12,13,15}, independent bright field and fluorescence imaging¹⁴ or single excitation wavelength capability^{16,17}. Some of the existing devices use an excitation power density of >10 mW/cm². Our devices operate at slightly lower power densities but are capable of operating at several excitation wavelengths, allowing independent imaging of a number of dyes. We present data acquired at two wavelengths: these have been tested to date, though a greater number is readily feasible.

2. METHODS AND THEORY

2.1 Device development

Excitation light is provided by 660 nm and 785 nm solid-state laser diodes capable of generating several hundred milliwatts of optical power from 100 μm diameter 0.22 NA multimode optical fibers. A custom-made fiber bundle terminated in a FC/PC connector combines outputs from multiple laser fibers. Up to 7 laser fibers can be coupled into a 1050 μm diameter bundle and more than one laser of the same wavelength can be used when higher powers are required. Visible light is generated using a white LED (i.e. a phosphor-coated blue LED). A 650 nm corner wavelength dichromatic mirror combines collimated LED white light and collimated bundle output light. An in-house developed achromatic objective focuses the resulting combined light into a 3-5 mm diameter spot at 0.5 NA (numerical aperture); this spot is located at the output port of the control unit (Figure 1A). Either 3 mm or 5 mm diameter liquid light guides send light to the widefield imager and the laparoscope excitation ports respectively. Because of the widely different étendues of the LED and laser sources, it is, strictly speaking, impossible to make the NAs and the areas identical: the use of a liquid-filled light guide is thus to be preferred, as it acts as a beam homogenizer.

The laparoscope imaging system is coupled to the eyepiece of a Storz Hopkins II 10 mm 0 degree rigid laparoscope (Figure 1B), although the system can be used with other similar laparoscopes. Both systems use the same type of miniaturized 1/3" format CCD color camera, modified to operate in both the visible and NIR. The camera uses a Sony Super HAD CCD II™ sensor¹⁸ to achieve a high level of sensitivity. It provides interlaced video (PAL standard) and allows integration of several seconds to be used, if required. Similarly, both systems use 25 mm focal length visible – NIR achromatic imaging lenses. Both lenses include a focusing system: for laparoscopy, this is manually set, while for widefield imaging, a motorized focusing arrangement is used.

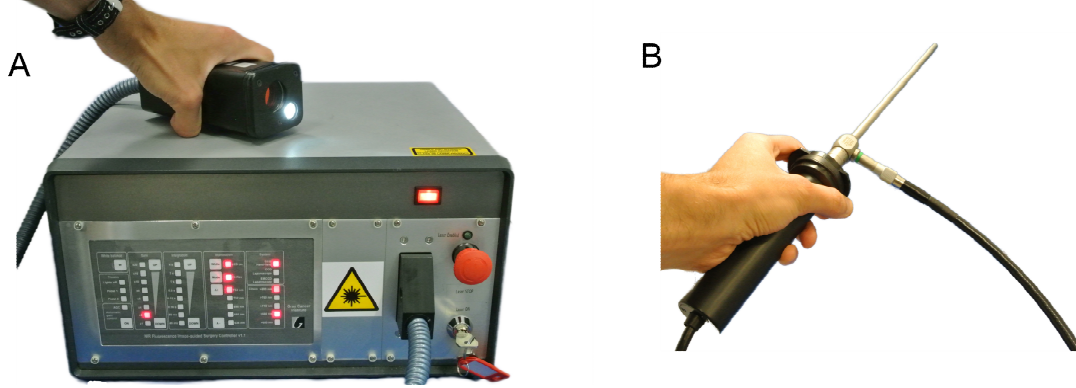


Figure 1: Imaging devices final design. (A) The control unit and the widefield imager connected to it through a combined optical-electrical umbilical connector. (B) Laparoscopic attachment used in conjunction with a rigid Storz Hopkins II 10 mm 0 degree laparoscope. The laparoscope uses a similar type of electrically-coded connector (not shown) that can be plugged into the common control unit, and allows fast device interchange.

2.2 Laparoscopic system characterization

One of the aims of the work presented here was to optically characterize the Storz Hopkins II 0 degree, 10 mm diameter laparoscope, generally used for abdominal keyhole surgery, with the aim of predicting imaging performance. Such information is not generally easily available, particularly so in the NIR. This information guided the development of the rest of the instrumentation.

A laparoscope imaging channel typically consists of an objective lens, a rod lens relay system¹⁹ and an eyepiece at the output. The light transmission power of the laparoscope is determined by its aperture (stop) and by the transmission of the optical elements. These have been individually determined experimentally to derive both the system f-number and, in effect, the system T-number²⁰. The ubiquitous f-number²¹ describes the aperture:

$$f/\# = \frac{f}{d} \quad (1)$$

where f is the focal length of the system and d the diameter of the entrance pupil. We determined the equivalent focal length f of the system by using the formula:

$$f = \frac{w_d s}{FOV} \quad (2)$$

where FOV is the diagonal field of view at a working distance w_d from the tip of the laparoscope as seen with an image sensor of diagonal dimension s . In our case $s = 6$ mm (1/3" format sensor). We measured the diameter of the entrance pupil d by imaging the front of the laparoscope using a separate FOV-calibrated imaging system. This f/1.4 system (working distance of ~50 mm) imaged the laparoscope pupil. This short working distance allowed imaging of the entrance pupil over a significant number of pixels (typically >2000) and thus reduced measurement errors. In addition, the high aperture and a short working distance provided a very shallow depth of field that resulted in a good estimation of both the pupil diameter and its position. Without changing imager position or focus, a ruler replaced the laparoscope and provided, when in focus, a conversion factor pixels/unit length.

We measured independently the optical transmission using the experimental setup shown in Figure 2. We illuminated the eyepiece with a small diameter (100-200 μ m) monochromatic, collimated light beam. Laser sources operating at five wavelengths were used to provide collimated monochromatic light, with wavelengths ranging from the visible to the near infrared (532, 660, 732, 785, 830 nm). Each laser was collimated independently and coupled to the input of a 10x Galilean beam expander (Thorlabs BE10M). Small diameter apertures were used at the output of the expander to produce a re-collimated beam of diameter much smaller than the laparoscope exit pupil. An XY translation stage (Thorlabs ST1XY) aligned apertures to the system axis, such that the input collimator, beam expander, laparoscope eyepiece and laparoscope imaging port were all concentric. The optical transmission was determined through measurement of the intensities of the beams entering the eyepiece and leaving the laparoscope tip. A large area photodiode detector measured the relative intensities of these beams.

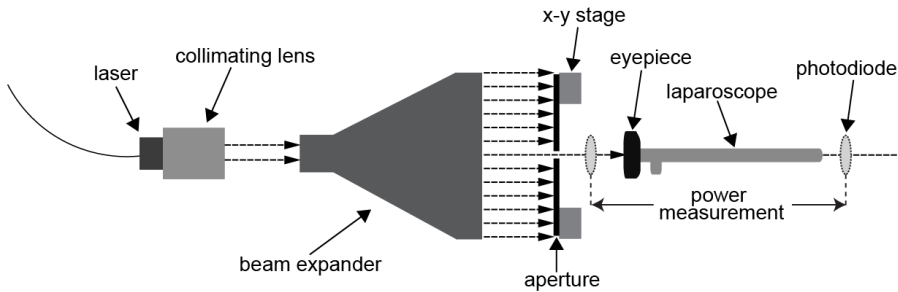


Figure 2: Experimental setup used for measuring light transmission through the laparoscope. Light transmission was determined by moving the photodiode between laparoscope input and output positions.

The transmission of the laparoscope was thus measured ‘in reverse’, using the eyepiece as the input, as it allowed us to perform the alignment in a simple manner and to use a collimated test beam of practical dimensions, in a portion of the system which would conventionally deliver nearly collimated light. Although this arrangement only determines the on-axis transmission, the transmission at other angles could be inferred when operating the laparoscope in its conventional imaging mode.

We used a similar experimental set-up, but with a larger expanded beam diameter (4.8 mm) to determine the transmission of the laparoscope illumination channel. This illumination channel consists of two parts: optical fiber bundles within the laparoscope and a flexible light guide to the laparoscope. We evaluated a Storz flexible fiber bundle guide as well as a liquid-filled light guide, the latter often used for increased throughput.

2.3 Fluorescence sensitivity

The next step was to validate the in-line measurements and to investigate whether we could predict the fluorescence detection performance of our laparoscopic system using the derived fluorescence collection efficiency. As reference, we used our widefield imager, where the performance was known. Since both systems used the same camera, the light gathering power was calculated by comparing the effective apertures of the two systems. The effective aperture of the widefield system was calculated from the lens infinity-set f/number; this was corrected for image and pupil magnification. The f/number of the laparoscope was calculated using Equation (1). Given the low image magnification ($m \sim 0.04$) of the laparoscope when used at a typical working distance of 100 mm, we considered this f/number to represent the effective aperture of the system.

Indocyanine green (ICG) dye is commonly used in FIGS procedures²², as it is a clinically-approved dye with negligible toxicity. As shown by previous studies, the fluorescence emission of ICG increases when it binds to plasma proteins²³. We therefore diluted ICG in a plasma-equivalent solution. We used the recipe described by Gashev *et. al.*²⁴ to produce an albumin-enriched physiological salt solution (APSS) and used this as the solvent. ICG was diluted at concentrations ranging from 20 μ M to 200 nM in 1 ml volume solutions. Further dilutions down to 7.5 nM were used to determine the detection limit of the widefield imager.

ICG:APSS was excited at 785 nm and 15 mW/cm², and used as a test sample to validate the performance of the laparoscope. Imaging was performed at working distances of 350 mm for the widefield system and 100 mm for the laparoscope. Relative sensitivity was calculated as a ratio of the average fluorescence intensities from equivalent sample imaged areas. For this purpose, video was digitized using a CCIR video-to-USB 8 bit resolution converter (The Imaging Source, DFG/USB2PROPCB). Data from >1000 pixels were typically used for intensity measurements. Image analysis was performed with ImageJ software (National Institutes of Health). Imaging results were compared with relative sensitivity calculated from the laparoscope transmission and f/number that we determined.

2.4 Intraoperative fluorescence imaging

We validated our devices *in vivo* in a feasibility study on sentinel lymph nodes detection in various gynecological cancers using ICG and Methylene blue (MB) fluorescent dyes. Patients with early stage vulvar, cervical and endometrial cancer were involved in the study. Following ethical approval of the study and informed patient consent, ICG and MB were injected peritumorally at concentrations of <1 mM and fluorescence assessed using the widefield imager and/or the laparoscope. The presence of the dye was assessed *ex vivo* using an in-house developed microscope²⁵, modified to include NIR laser illumination.

3. RESULTS

3.1 Device testing

The imaging devices delivered typically $\sim 1\text{-}2 \text{ mW/cm}^2$ of white light illumination. The widefield imager delivered this at a working distance of 350 mm while the working distance of the laparoscope was typically 100 mm when delivering a similar white light power density. Fluorescence excitation power density was $\sim 3 \text{ mW/cm}^2$ and $\sim 7 \text{ mW/cm}^2$ at 660 nm and 785 nm respectively. The angular field of view of the widefield imager was $\sim \pm 6.5$ degrees, equivalent to an imaged area of $\sim 100 \text{ cm}^2$, while the angular field of view of the laparoscope was $\sim \pm 37$ degrees, equivalent to an imaged area of $\sim 150 \text{ cm}^2$. The widefield imager was developed to provide a usefully small surgical field while maintaining maximum permissible exposure (MPE) power levels. In order to decrease the likelihood of the accidental exposure, a tilt switch acts as an interlock, allowing illumination only when the hand-held device is pointed downwards.

We tested the ability of this technology to image bright field and fluorescence using a sample containing 100 nM of indocyanine green (ICG) dye (Pulsion Medical Systems, Munich, Germany) in a capillary tube (diameter 500 μm) and a color chart (RezChecker, Edmund Optics 87-423). Figure 3(A-C) shows examples of simultaneous bright field and fluorescence detection of a sample of ICG at different camera integration times. Variations of image field of view with distance and resulting power density changes are shown in Figure 3D.

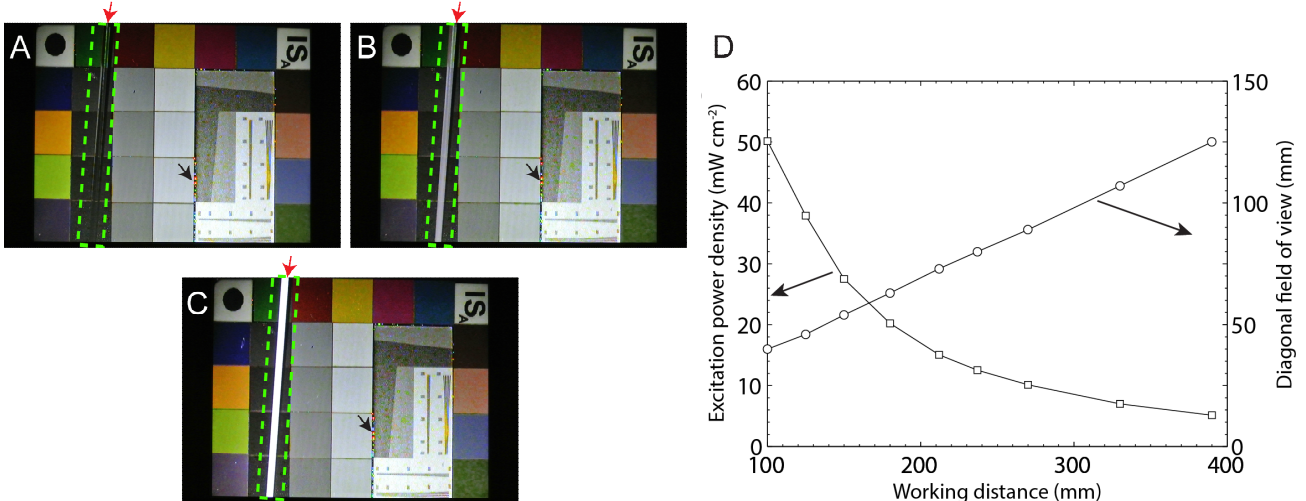


Figure 3: Imaging results obtained with the widefield imager imaging a color chart and a 100 nM ICG-filled capillary tube, outlined by dotted rectangle (red arrows). (A) Bright field image (laser OFF, 4 ms exposure). (B) ICG fluorescence (785 nm laser ON, 40 ms exposure). (C) ICG fluorescence (785 nm laser ON, 320 ms exposure). A similar result is obtained when camera gain is increased (not shown here). Fluorescence excitation power density: 16 mW/cm^2 . Working distance: 200 mm. An f/5.6 imager aperture provides a good depth of field. The Moiré patterns visible on A, B, C (black arrows) could be removed with an MTF anti-aliasing filter in front of the image sensor. (D) Widefield imager 785 nm excitation power density and diagonal field of view as a function of working distance.

3.2 Laparoscope sensitivity determination

We calculated the field of view of the laparoscopic system and, using equation (2), measured the effective focal length to be 4.02 ± 0.01 mm. By using the approach described in §2.2, the entrance pupil was measured to have a diameter 0.451 ± 0.003 mm (Figure 4A). This suggests an f-number of 8.91 ± 0.06 . Figure 4B shows absolute spectral transmission of the laparoscope detection channel as measured with the setup described in §2.2. The transmission decreases significantly in NIR portion of the optical spectrum. The transmission of the laparoscope light delivery fibers was found to be independent of light wavelength, over the range 532 nm - 830 nm. However, we tested two Storz laparoscopes, nominally identical, i.e. with the same part number, but found that the transmission varied between $\sim 31\%$ and $\sim 37\%$. It is probable that even larger variations exist from device-to-device, resulting from a combination of manufacturing tolerances and, more likely, from sterilization history.

We measured the transmission of the flexible light guides used to transport light to the illumination channel. Fiber bundles (transmission ~78%) are more widely used in conjunction with laparoscopes and have the advantages of being very flexible and readily sterilized. However, liquid-filled light guides exhibit higher throughput (transmission ~85%).

Following spectroscopic measurement of ICG:APSS in which the emission peak was determined (data not shown), we used the 830 nm transmission value in Figure 4B to calculate the laparoscope detection efficiency. This was validated by imaging ICG:APSS samples using a widefield and laparoscopic systems. Relative sensitivity calculations and experimental measurements were performed as described in §2.3 and the results shown in Figure 5A. These data suggest that, for a similar field of view, but at working distances appropriate to the two systems (100 and 350 mm) the laparoscope has the same apparent sensitivity as a widefield imaging system operating at $\sim f/20$.

Figure 5B shows changes of ICG fluorescence emission as a function of concentration. ICG is well known to exhibit extremely non-linear properties²⁶, confirmed by these measurements. We also show, in the inset of Figure 5B, how the signal-to-noise ratio, though acceptable, dramatically decreases with laparoscopy imaging of low ICG concentrations.

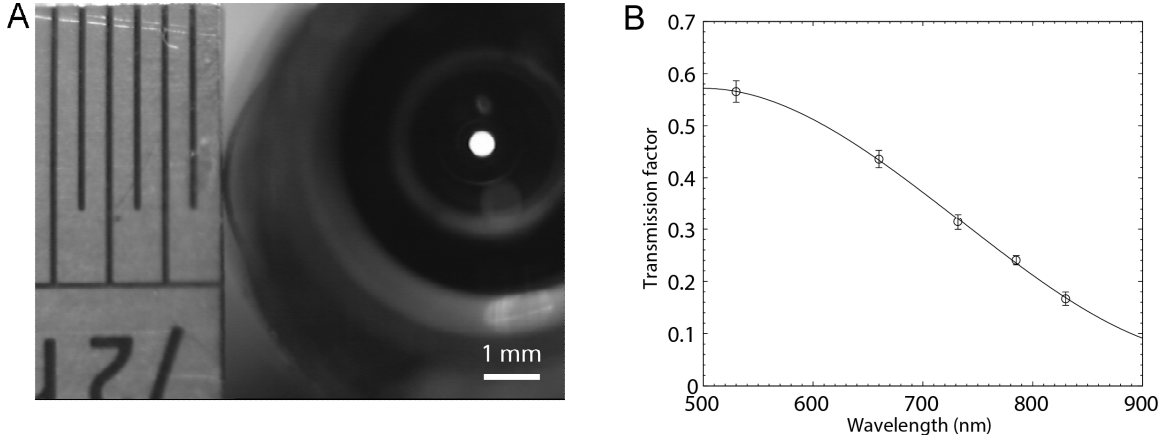


Figure 4: (A) Image of the entrance pupil of the laparoscope. (B) Absolute transmission of the laparoscope detection system. Error bars represent the standard deviation of measurements performed in triplicate, using different laser spot sizes. All measurement were made as described in §2.2.

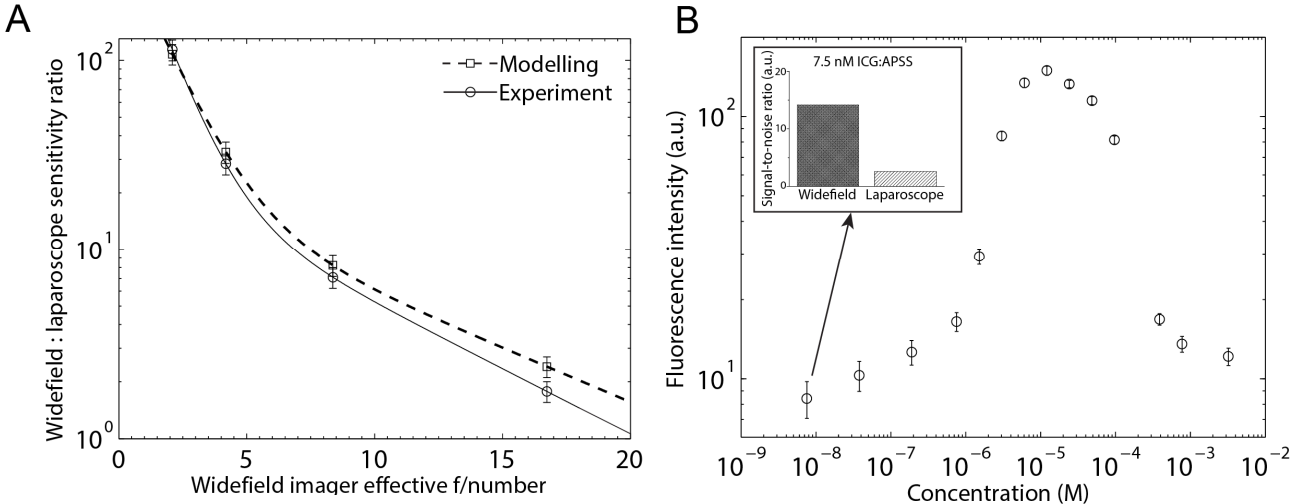


Figure 5: (A) Measurement-derived (dashed curve) and experimentally derived (solid curve) sensitivity ratio widefield:laparoscope for different apertures of the widefield system lens. Error bars in the experiment data represent the standard deviation of experiments conducted in triplicate using different concentrations of ICG:APSS (20 μ M, 2 μ M and 200 nM). (B) Fluorescence intensity of ICG:APSS as a function of concentration, using the widefield imager. Inset: Image signal-to-noise ratio when imaging the lowest concentration (7.5 nM) using the widefield imager and the laparoscope camera system at 320 and 1000 ms exposure time respectively.

3.3 Clinical validation

We validated both widefield and laparoscopic systems *in vivo* during a feasibility study involving sentinel lymph node detection in gynecological cancer patients. Lymphatic channels and lymph nodes were visualized using exposure times ranging from 40 ms to 320 ms, depending on the type of imaging device and the tissue depth of the fluorescence source (Figure 6). White light reflectance imaging of the surgical field was displayed simultaneously with fluorescence. Both ICG and MB could be detected by switching between 660 and 785 nm excitation.

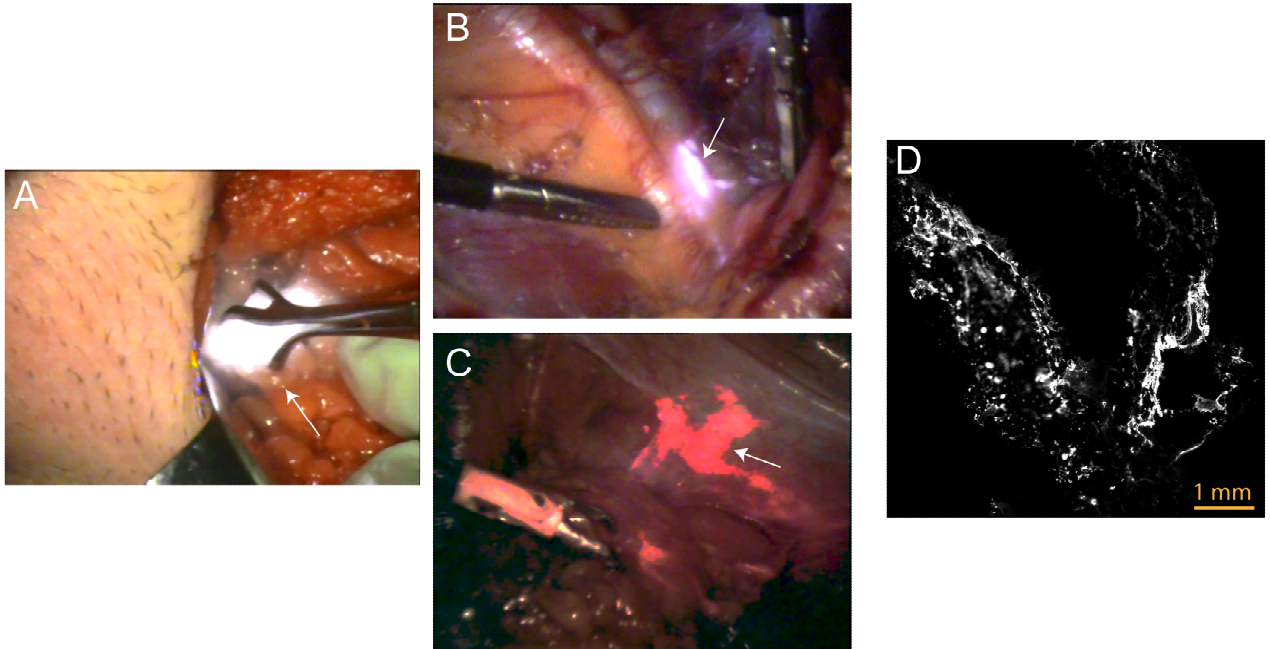


Figure 6: (A-C) Frames captured from surgery recordings. (A) Intra-operative lymph node resection in vulvar cancer imaged with the widefield system. Bright field and fluorescence emission (white arrow) displayed simultaneously. Camera exposure time: 40 ms. (B, C) Fluorescence laparoscopy with ICG (B) and MB (C) dyes using 785 nm and 660 nm excitation respectively in a patient with endometrial cancer. Integration time: 80 ms. (D) Exemplar image of a slice of lymph node tissue captured with a NIR fluorescence microscope.

4. DISCUSSION

We have characterized the optical performance of a Storz Hopkins II rigid laparoscope. We have determined the system collection efficiency by measuring the light gathering power of the optical system (f/number) and the absolute optical losses. To our knowledge, this is the first time that the characteristics of both the imaging and the excitation channels of a laparoscope were determined experimentally. The laparoscope imaging channel is equivalent to a \sim f/8.9 aperture but with an overall light transmission that drops from \sim 55% in the visible to \sim 18% at 830 nm. The measurements suggest that the detection sensitivity for laparoscopic imaging is \sim 20 times worse than widefield imaging at f/5.6. This sensitivity loss becomes even greater when widefield imaging is performed at a lower f/number (\sim 120x at f/2), though the resulting poor depth of field makes use hard, particularly with small area imaging chips. We find that f/5.6 is appropriate for a practical hand-held device.

Fluorescence image-guided surgery is rapidly emerging as a complementary technique to conventional white light reflectance imaging. Past attempts by others, using two or more cameras to image white light and fluorescence independently^{12,13} have shown some advantages over the system described here when used as widefield imaging devices. However, such systems are bulky and, in general, not compatible with laparoscopy applications. We described here the testing and application of novel, low cost devices suitable for fluorescence image guided surgery. They are appropriate for open surgery applications (widefield imager) and for keyhole surgical applications (in conjunction with a standard laparoscope). We have used them successfully in a clinical study aimed at detection of lymph nodes in gynecological cancers, using indocyanine green and Methylene blue non-specific dyes. To our knowledge, our system is the first that

allows use of either a widefield imaging head or a laparoscope imager with the same control unit. In contrast to other existing devices, we are able to perform white light reflectance imaging and multispectral fluorescence imaging simultaneously using a single color CCD camera, without the need of software image overlays, as required by systems employing multiple cameras. Our system components are miniaturized and lightweight, and are optimized for handheld operation. Successful near real-time fluorescence imaging was possible with both widefield and laparoscopic systems. The principle limitation of our current devices is poorer spatial resolution than that possible with the best white-light only imaging systems. We are working on integrating a megapixel resolution imager to rectify this issue, along with further developments of illumination/excitation sources. We anticipate that this technology will find use in a variety of surgical procedures and that it can play a role in the emerging field of clinical fluorescence molecular imaging.

ACKNOWLEDGEMENTS

The authors would like to thank S. Kennedy for suggesting the need to explore FIGS instrumentation, R. G. Newman, J. Prentice, G. Shortland and P. Barber for technical assistance. This work was supported by Oxford Cancer Imaging Centre Grant (Programme grant C5255/A16466), with funding from Cancer Research UK, EPSRC, Oxford Biomedical Research Centre, the National Institute of Health Research and the Medical Research Council. We thank the Early Phase Clinical Trials Unit and The Gynaecological Oncology Multidisciplinary Team at Oxford for assistance with recruiting patients. Last but not least, we thank the patients who participated in the study partially described here.

REFERENCES

- [1] National Cancer Institute. SEER cancer statistics review, 1975–2005, [http://seer.cancer.gov/csr/1975_2005_\(2008\).](http://seer.cancer.gov/csr/1975_2005_(2008).)
- [2] Keereweer, S., Kerrebijn, J.D., van Driel, P.B., Xie, B., Kaijzel, E.L., Snoeks, T.J., Que, I., Huttelman, M., van der Vorst, J.R., Mieog, J.S., Vahrmeijer, A.L., van de Velde, C.J., Baatenburg de Jong, R.J., Löwik, C.W., "Optical Image-guided Surgery – where do we stand" Mol. Imaging Biol. 13, 199-207 (2011).
- [3] van Dam, G.M., Themelis, G., Crane, L.M., Harlaar, N.J., Pleijhuis, R.G., Kelder, W., Sarantopoulos, A., de Jong, J.S., Arts, H.J., van der Zee, A.G., Bart, J., Low, P.S., Ntziachristos, V., "Intraoperative tumor-specific fluorescence imaging in ovarian cancer by folate receptor- α targeting: first in-human results", Nat. Med., 17(10), 1315-9 (2011).
- [4] Kitai T., Inomoto T., Miwa M., Shikayama T., "Fluorescence navigation with indocyanine green for detecting sentinel lymph nodes in breast cancer", Breast Cancer, 12(3), 211-5 (2005).
- [5] Vahrmeijer, A.L., Huttelman, M., van der Vorst, J.R., van de Velde, C.J.H. and Frangioni, J.V., "Image-guided cancer surgery using near-infrared fluorescence", Nat. Rev. Clin. Oncol., 10, 507–518 (2013).
- [6] Liu, Z., Miller, S.J., Joshi, B.P., Wang, T.D., "In vivo targeting of colonic dysplasia on fluorescence endoscopy with near-infrared octapeptide", Gut, 62(3), 395-403 (2013).
- [7] Harlaar, N.J., Kelder, W., Sarantopoulos, A., Bart, J., Themelis, G., van Dam, G.M., Ntziachristos, V., "Real-time near infrared fluorescence (NIRF) intra-operative imaging in ovarian cancer using an $\alpha(v)\beta(3)$ - integrin targeted agent", Gynecol. Oncol., 128(3), 590-5 (2013).
- [8] Metildi, C.A., Hoffman, R.M., Bouvet, M., "Fluorescence-guided surgery and fluorescence laparoscopy for gastrointestinal cancers in clinically-relevant mouse models", Gastroenterol. Res. Pract., 2013, 290634 (2013).
- [9] Nguyen, Q.T., Olson, E.S., Aguilera, T.A., Jiang, T., Scadeng, M., Ellies, L.G., Tsien, R.Y., "Surgery with molecular fluorescence imaging using activatable cell-penetrating peptides decreases residual cancer and improves survival", PNAS, 107(9) (2010).
- [10] Gershenwald, J.E., Thompson, W., Mansfield, P.F., Lee, J.E., Colome, M.I., Tseng, C.H., Lee, J.J., Balch, C.M., Reintgen, D.S., Ross, M.I., "Multi-institutional melanoma lymphatic mapping experience: the prognostic value of sentinel lymph node status in 612 stage I or II melanoma patients", J. Clin. Oncol., 17(3), 976-83 (1999).
- [11] Veronesi, U., Paganelli, G., Viale, G., Galimberti, V., Luini, A., Zurruda, S., Robertson, C., Sacchini, V., Veronesi, P., Orvieto, E., De Cicco, C., Intra, M., Tosi, G., Scarpa, D., "Sentinel lymph node biopsy and axillary dissection in breast cancer: results in a large series", J. Natl. Cancer Inst., 91(4), 368-73 (1999).

- [12] Themelis, G., Jung, S.J., Kwang-Sup, S., Schulz, R., Ntziachristos, V., “Real-time intraoperative fluorescence imaging system using light-absorption correction”, *J. Biomed. Opt.*, 14(6), 064012 (2009).
- [13] Troyan S.L., Kianzad V., Gibbs-Strauss S.L., Gioux S., Matsui A., Oketokoun R., Ngo L., Khamene A., Azar F., Frangioni J.V., “The FLARE intraoperative near-infrared fluorescence imaging system: a first-in-human clinical trial in breast cancer sentinel lymph node mapping”, *Ann. Surg. Oncol.*, 16(10), 2943-52 (2009).
- [14] Gioux, S., Coutard, J.G., Berger, M., Grateau, H., Josserand, V., Keramidas, M., Righini, C., Coll, J.L., Dinten, J.M. “FluoSTIC: miniaturized fluorescence image-guided surgery system”, *J. Biomed. Opt.*, 17(10), 106014 (2012).
- [15] Glatz, J., Varga, J., Garcia-Allende, P.B., Koch, M., Greten, F.R., Ntziachristos, V., “Concurrent video-rate color and near-infrared fluorescence laparoscopy”, *J. Biomed. Opt.*, 18(10), 101302 (2013).
- [16] Gray, D.C., Kim, E.M., Cotero, V.E., Bajaj, A., Staudinger, V.P., Hehir, C.A., Yazdanfar, S., “Dual-mode laparoscopic fluorescence image-guided surgery using a single camera”, *Biomed. Opt. Express*, 3(8), 1880-90 (2012).
- [17] Liu, Y., Njuguna, R., Matthews, T., Akers, W.J., Sudlow, G.P., Mondal, S., Tang, R., Gruev, V., Achilefu, S., “Near-infrared fluorescence goggle system with complementary metal-oxide-semiconductor imaging sensor and see-through display”, *J. Biomed. Opt.*, 18(10), 101303 (2013).
- [18] http://www.sony.net/Products/SC-HP/cx_news/vol52/pdf/featuring52.pdf.
- [19] Hopkins, H.H., “Optical system having cylindrical rod-like lenses”, US Patent: US3257902 A (1966).
- [20] Ray, S.F., “Applied photographic optics”, Focal press, 128-129 (2002).
- [21] Born M., Wolf E., “Principles of Optics, Electromagnetic Theory of Propagation, Interference and Diffraction of Light – 7th Edition”, Cambridge University Press, 200-201 (1999).
- [22] Alander, J.T., Kaartinen, I., Laakso, A., Pätilä, T., Spillmann, T., Tuchin, V.V., Venermo, M., Välisuo, P., “A review of indocyanine green fluorescent imaging in surgery”, *Int. J. Biomed. Imaging*, 2012, 940585 (2012).
- [23] Weiler M., Kassis T., Dixon J.B., “Sensitivity analysis of near-infrared functional lymphatic imaging”, *J. Biomed. Opt.*, 17(6), 066019 (2012).
- [24] Gashev A.A., Davis M.J., Zawieja D.C., “Inhibition of the active lymph pump by flow in rat mesenteric lymphatics and thoracic duct”, *J. Physiol.*, 540(Pt 3), 1023-37 (2002).
- [25] Barber, P.R., Tullis, I.D.C., Pierce, G.P., Newman, R.G., Prentice, J., Rowley, M., Matthews, D.R., Ameer-Beg, S.M., Vojnovic, B., “The Gray Institute ‘Open’ High-Content, Fluorescence Lifetime Microscopes”, *J. Microsc.*, 251(2), 154-167 (2013).
- [26] Maarek, J.M., Holschneider, D.P., Harimoto, J., “Fluorescence of indocyanine green in blood: intensity dependence on concentration and stabilization with sodium polyaspartate”, *J. Photochem. Photobiol. B*, 65(2-3), 157-64 (2001).